Accepted Article Preview: Published ahead of advance online publication

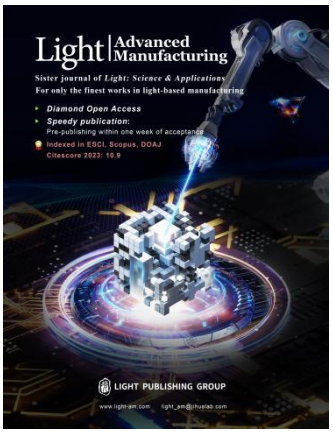

Full-parallax High-resolution Light Field 3D Display Based on Time-sequential Polarization Liquid Crystal Lens Array

Xue-Rui Wen, Yan Xing, Xing-Yu Lin, Yi-Jian Liu, Wei-Ze Li, Fan Chu and Qiong-Hua Wang

Cite this article as: Xue-Rui Wen, Yan Xing, Xing-Yu Lin, Yi-Jian Liu, Wei-Ze Li, Fan Chu and Qiong-Hua Wang. Full-parallax High-resolution Light Field 3D Display Based on Time-sequential Polarization Liquid Crystal Lens Array. *Light: Advanced Manufacturing* accepted article preview article preview 17 April, 2026; doi: 10.37188/lam.2026.069

Received 08 June 2025; revised 23 March 2026; accepted 9 April 2026;
Accepted article preview online 17 April 2026

Full-parallax High-resolution Light Field 3D Display Based on Time-sequential Polarization Liquid Crystal Lens Array

Xue-Rui Wen,† Yan Xing,† Xing-Yu Lin, Yi-Jian Liu, Wei-Ze Li, Fan Chu *, and Qiong-Hua Wang *

School of Instrumentation and Optoelectronic Engineering, Beihang University, Beijing 100191, China

*chufan@buaa.edu.cn

*qionghua@buaa.edu.cn

†These authors contributed equally to this work.

Abstract

High-performance three-dimensional (3D) display technology has been regarded as the future of display technology. However, improving the resolution of the light field 3D display while ensuring full parallax has been a challenge. A light field 3D display based on time-sequential polarization liquid crystal (LC) lens array is proposed to achieve full parallax and high-resolution display. An analysis is conducted on the effect of the frequency response of the lens array on the resolution, and a time-sequential polarization LC lens array is proposed, which improves resolution compared to a microlens array or a lenticular lens array. In addition, the time-sequential polarization LC lens array focuses light in different directions by switching the polarization direction of the incident light. Combined with the parallax-separated pixel encoding method, the proposed light field 3D display achieves a resolution of 1732×1265 and realizes a full parallax with a horizontal and vertical viewing angle of 12.5° by time-division multiplexing. The global resolution is higher than the light field 3D displays based on a lenticular array and a microlens array with the same lens parameters. The polarization conversion layer in the proposed LC lens array can achieve a switching rate of about 208 Hz, which ensures the feasibility of a high frame rate display.

Keywords: 3D display, light field 3D display, high-resolution, optical imaging, liquid crystal.

Introduction

Three-dimensional (3D) display is one of the most promising displays that provide realistic 3D images and have a great need and application in advertising, entertainment, military, medical, and other areas. The light field 3D display has superior advantages such as providing all depth cues, correct geometric occlusion, and the avoidance of vergence-accommodation conflict, which is regarded as one of the most promising 3D display technologies[1-4]. The light field 3D display refers to the display technology

that reconstructs the 3D image by completely recreating the light field distribution. The current mainstream technologies of light field 3D display include integral imaging 3D display[5-7], super-multi-view 3D display[8, 9], compressive light field 3D display[10, 11], etc. The integral imaging 3D display employs the microlens array to modulate the light emitted from the two-dimensional (2D) display, providing a full parallax[12]. However, this approach suffers from a lack of resolution because of the presence of spacing in the microlens array. The super-multi-view 3D display utilizes a lenticular lens array to reconstruct the 3D image, enabling the reception of multiple viewpoints within the range of a single eye[13]. This approach can achieve a more realistic and natural 3D image reconstruction. Nevertheless, it also has limitations, as it results in a one-dimensional parallax. The compressive light field 3D display achieves light field reconstruction through the codesign of optical elements and computational-processing algorithms, ensuring that fewer display pixels are necessary to emit a given light field than a direct optical solution would require[14]. However, compressive light field displays also result in significant brightness attenuation, and multi-layer optical elements entail considerable structural complexity. Consequently, i the above-mentioned displays possess inherent drawbacks.

The aforementioned drawbacks are derived from the limited total amount of 2D information, which constrains the simultaneous enhancement of multiple 3D display parameters. Researchers utilize space-division multiplexing or time-division multiplexing schemes to enhance the 2D information capacity and therefore improve the resolution and other 3D display parameters[15-17]. The liquid crystal (LC) offers the advantages of polarity-sensitive switching and anisotropic characteristics, and its application in space-time multiplexing represents a promising approach to enhancing the performance of 3D displays[18-29]. A method to reduce resolution loss has been proposed that uses 32 time-sequentially opened ferroelectric liquid crystal light valve arrays to display images from different directions.[30]. This work presents a solution that achieves independent control of 32 light valves without inversion, thereby reducing crosstalk and improving the equivalent 3D resolution. However, the final 3D resolution still needs to be improved due to the suboptimal design of the microlens array and the considerable imaging aberration. A 2D/3D mixed frontal projection system based on integral imaging has been proposed which employs an LC microlens array and a quarter-wave retarding film with pinholes to achieve free switching between 2D, 3D, and 2D/3D mixed display states[31]. However, the attenuation of light intensity and lack of clarity are still drawbacks. The fabrication of new LC 2D displays represents an additional avenue for enhancing the total amount of 2D information. A series of three novel LC mixtures have been proposed as potential solutions for phase modulators utilized in augmented reality displays[32]. These LC mixtures feature highly birefringent, achieving a thin cell gap with a 240 Hz refresh rate, a moderate dielectric anisotropy at 5 V operating voltage, acceptable resistivity and UV stability, and a wide vector range. The experimental demonstration of these LC mixtures in mixed-mode twist nematic Liquid-Crystal-on-Silicon amplitude modulators has shown that they can achieve an operating frequency of 1 kHz, which helps to realize 3D displays with high refresh rates. It is evident that LC has the potential to significantly enhance the performance of 3D displays.

We propose a full-parallax high-resolution light field 3D display based on the time-sequential polarization LC lens array. The polarization direction of the light emitted from the 2D display is controlled through the polarization conversion layer (PCL), and it is selectively refracted by the LC lens array. A parallax-separated pixel encoding method is used to synthesize element image arrays (EIAs) with horizontal and vertical parallaxes, respectively, and the 3D displays with the horizontal and vertical parallaxes are realized by the time-division multiplexing technique. The effects of the frequency responses of different types of lens arrays on the 3D display resolution are analyzed and

compared, and a prototype of light field 3D display based on the time-sequential polarization LC lens array is developed. The reconstructed 3D images of the proposed 3D display have a higher global resolution compared to that of the light field 3D display based on the conventional lenticular lens array and microlens array.

Structure and operating principle

Principle of the proposed light field 3D display

Fig. 1a illustrates the configuration of the full-parallax high-resolution light field 3D display, which comprises a 2D display, and an orthogonal LC lens array with a PCL. Fig. 1b shows the cross-sectional view of the orthogonal LC lens array with a PCL in both the voltage-off and voltage-on states. The orthogonal LC lens array is divided into two parts: the top LC lens array and the bottom LC lens array. The two different parts are separated from each other by a substrate. The top and bottom LC lens arrays have the same "substrate - LC molecules - substrate" structure. In a single layer of the lens array, the substrate above the LC molecules has planar electrodes, while the substrate below is coated with periodically rectangular electrodes as the driving electrodes. The two rectangular electrodes are arranged in orthogonal directions in the top and bottom lens arrays, and the LC molecules are aligned in the directions that are perpendicular to the corresponding rectangular electrodes, which enables both lens arrays to have an orthogonal direction focusing effect. d is the thickness of the LC layer, w is the width of the rectangular electrodes, and l is the distance between the rectangular electrodes. It should be noted that the orthogonal LC lens array is always in operation.

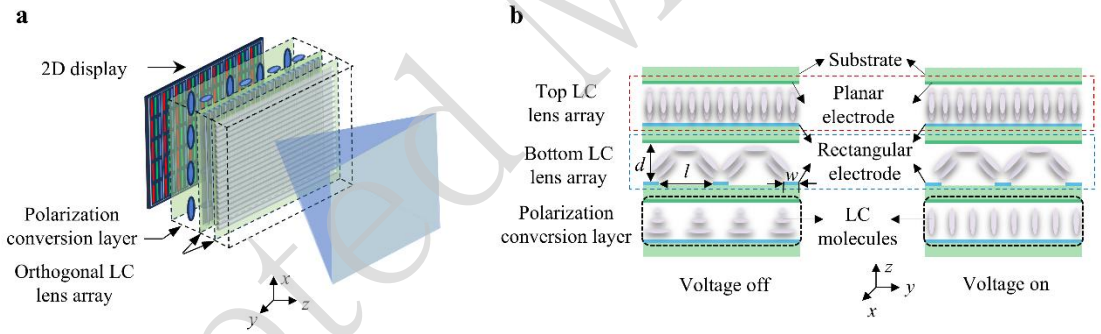

Fig. 1 Principle of the proposed light field 3D display. a Schematic diagram of the proposed light field 3D display. **b** Cross-sectional view of the LC lens array with a PCL at different voltage states. The top and bottom LC lens arrays are represented by red and blue dashed lines, respectively.

The 2D display emits linearly polarized light, which is rotated in the polarization direction after passing through the PCL. The light is refracted by the corresponding LC lens array, thereby reconstructing the 3D image. It is assumed that the light emitted from the 2D display is polarized in the vertical direction. In Fig. 2a, when the PCL layer is in the voltage-off state, it will rotate the incident linearly polarized light by 90°. This results in the polarization of the light being in the horizontal direction, which is perpendicular to the LC molecules in the top LC lens array. Consequently, the outgoing linearly polarized light passing through the top LC lens array can be seen as an ordinary wave, making the top LC lens array equivalent to a transparent glass plate. At this point, in terms of the bottom LC lens array, the polarization direction of the incident linearly polarized light is parallel to the alignment direction of the LC molecules, and it can be regarded as an extraordinary wave when it

passes through the bottom LC lens array, resulting a focusing effect. Thus, the proposed display presents a 3D display with horizontal parallax. When the PCL layer is in the voltage-on state, light passes through the PCL and the direction of polarization remains constant. The polarization direction of the light is perpendicular to the direction of the LC molecules in the bottom LC lens array, which is equivalent to a transparent glass at this time. The light passes through the bottom lens array and is refracted by the top LC lens array, thus presenting a 3D display with vertical parallax, as shown in Fig. 2b.

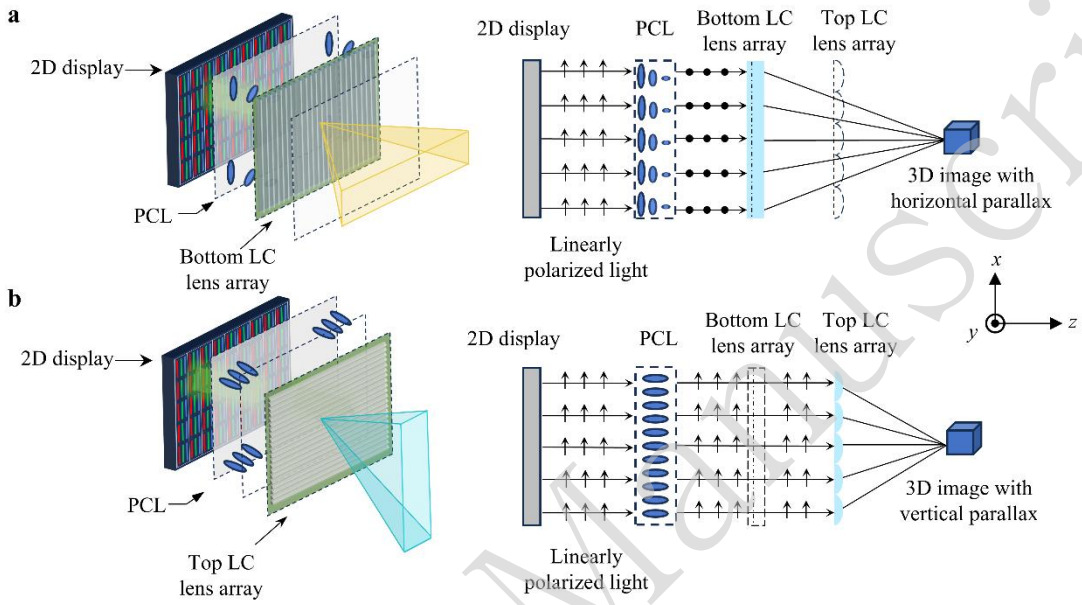

Fig. 2 Schematic diagram of the proposed light field 3D display for reconstructing 3D images at different voltage states. **a** The proposed light field 3D display in voltage-off state. **b** The proposed light field 3D display in voltage-on states.

As a linearly polarized light beam is incident parallel to the alignment direction of the LC molecules, the effective refractive index is expressed as[33, 34]

$$n_{\mathrm{eff}}(\theta)=n_o n_e \Big/ \left(n_o^2 \sin^2\theta + n_e^2 \cos^2\theta\right)^{1/2} \tag{1}$$

where n_e and n_o are the extraordinary and ordinary refractive indices of the LC layer, respectively. θ is the angle between the incident direction of polarized light and the LC director. The relationship between the focal length and the refractive index difference at the same time is given by

$$f=\frac{r^2}{2\delta n d} \tag{2}$$

where r is the effective half pitch of each LC lens, δn is the refractive index difference between the center and edge of the lens array, and d is the thickness of the LC layer.

Frequency response of proposed LC lens array

In the reconstruction process of light field 3D displays, the LC lens array modulates the light from the 2D display to reconstruct the 3D image. The presence of aberration in the lens array results in a loss of information as the light passes through the lens array. Optical design techniques are commonly employed to optimize the LC lens array to reduce information loss[35]. However, there is an upper-performance limit to optimizing the lens array because the frequency response of the lens array

is similar to low-pass filters in imaging systems, which cannot transmit information at high frequencies.

The frequency response of the lens array is generally used to characterize the information about the light that can be transmitted by the lens array since it characterizes the smallest detail that can be resolved by the lens array. Optimizing the frequency response of the lens array to transmit light information at higher frequencies is beneficial to improving the resolution of the reconstructed 3D image. A comparison is conducted between the frequency response of the proposed LC lens array with that of a microlens array and a lenticular lens array. In the analysis of the spatial frequency of information transmission, a transfer function is employed to describe the modulation of the spatial frequency of the information by the lens arrays. The lenticular lens is characterized by the ability to focus in one direction. Consequently, the transfer function of a lenticular lens usually has a low-pass characteristic in one direction and a full-pass characteristic in the other direction. The transfer function $H_{\text{lenticular\_lens}}$ of a lenticular lens can be expressed as

$$H_{\text{lenticular\_lens}}(u,v)=\begin{cases}1, |u|\le D\\ 0, |u|>D\end{cases} \quad \text{or} \quad H_{\text{lenticular\_lens}}(u,v)=\begin{cases}1, |v|\le D\\ 0, |v|>D\end{cases} \tag{3}$$

where u and v denote the frequency values in horizontal and vertical directions, respectively. D denotes the cut-off frequency. The microlens array has the ability to modulate in two directions and realize the full-parallax 3D display. The transfer function $H_{\text{microlens}}$ of a microlens can be expressed as

$$H_{\text{microlens}}(u,v)=\begin{cases}1, \sqrt{u^2+v^2}\le D\\ 0, \sqrt{u^2+v^2}>D\end{cases} \tag{4}$$

In terms of the proposed LC lens array, the operation process can be divided into two states. When the PCL is in a voltage-off state, the light traverses the bottom LC lens array to reconstruct the 3D image with horizontal parallax. When the PCL is in a voltage-on state, the light traverses the top LC lens array to reconstruct the 3D image with vertical parallax. Therefore, the transfer function $H_{\text{proposed\_lens}}$ of the proposed LC lens array is expressed as

$$H_{\text{proposed\_lens}}(u,v)=\begin{cases}1, |u|\le D_u\\ 0, |u|>D_u\end{cases} \qquad t = t_{\text{off}} \tag{5}$$

$$H_{\text{proposed\_lens}}(u,v)=\begin{cases}1, |v|\le D_v\\ 0, |v|>D_v\end{cases} \qquad t = t_{\text{on}} \tag{6}$$

where t_{off} and t_{on} denote the moments when the voltage is on and off, respectively. D_u denotes the horizontal cut-off frequency and D_v denotes the vertical cut-off frequency.

A lens array is a structure comprising multiple element lenses, each of which is capable of light modulation. The transfer function $H_{\text{lenticular\_lensarray}}$ of a lenticular lens array with a horizontal period can be expressed as

$$H_{\text{lenticular\_lensarray}}(u,v)=\sum_{n=-\infty}^{\infty} H_{\text{lenticular\_lens}}(u-nP,v) \tag{7}$$

where P denotes the pitch of the lenticular lens array and n denotes the number of periods of the lenticular lens array. In the case of the microlens array, it is periodically distributed in both horizontal and vertical directions. The transfer function of the microlens array $H_{\text{microlens\_array}}$ can be expressed as

$$H_{\text{microlens\_array}}(u,v)=\sum_{m=-\infty}^{\infty}\sum_{n=-\infty}^{\infty}H_{\text{microlens}}(u-nP_u,v-mP_v) \tag{8}$$

where P_u and P_v denote the pitch of the microlens array in horizontal and vertical directions, respectively. n and m denote the number of periods of the microlens array in horizontal and vertical directions, respectively. For the proposed LC lens array with the same pitches as the microlens array in both horizontal and vertical directions, the transfer function $H_{\text{proposed\_lensarray}}$ is expressed as

$$H_{\text{proposed\_lensarray}}(u,v)=\sum_{t=-\infty}^{\infty}\sum_{m=-\infty}^{\infty}\sum_{n=-\infty}^{\infty}H_{\text{proposed\_lens}}(u-nP_u,v-mP_v) \tag{9}$$

The transfer function images of three types of lens arrays in the frequency domain can be obtained by Equations (7)-(9), as shown in Fig. 3a. The white part indicates frequencies that pass through the lens array and the black part indicates frequencies that cannot pass through the lens array. The transfer function image of the lenticular lens array is represented by multiple pass bands in the horizontal direction while there is no restriction in the vertical direction. In contrast, the transfer function image of the microlens array is characterized by multiple circular pass regions. For the proposed LC lens array, the transfer function image is represented by multiple black regions with the most white regions, which proves that most of the frequencies of light rays can pass through the proposed LC lens array. The comparison of the three transfer function images reveals that the proposed LC lens array is capable of transmitting information at highest frequencies with the same cut-off frequency.

In accordance with the imaging principle of the lens array, the reconstructed 3D image in the frequency domain can be expressed as the product of the EIA which has been converted to the frequency domain and the transfer function of the lens array. The frequency domain signal F_{3D} of the reconstructed 3D image can be expressed as

$$F_{3D}(u,v)=F_{\text{EIA}}(u,v)\cdot H_{\text{lensarray}} \tag{10}$$

where F_{EIA} represents the frequency domain distribution of the EIA after Fourier transformation and $H_{\text{lensarray}}$ denotes the transfer function of three types of lens arrays. The frequency domain signal F_{3D} is then converted into the spatial domain distribution E_{3D} of the 3D image by the inverse Fourier transform as

$$E_{3D}(x,y)=\iint F_{3D}(u,v)e^{j2\pi(ux+vy)}dudv \tag{11}$$

The modulation effects of the lenticular lens array and microlens array for different frequency signals are first analyzed. Fig. 3b shows the results of modulating the origin image using the lenticular lens array with a horizontal period and microlens array, respectively. The origin image contains multiple black and white line pairs with different frequencies of 3 and 5 in both directions, which are used to simulate the periodic structure image in EIA as well as the images corresponding to the main body and detail. The value of the frequency represents the number of times the line pair occurs in the whole image. Low frequency pairs correspond to the main body information, and high-frequency pairs correspond to the detail information. The cut-off frequency of both the lenticular lens and the microlens is 4. It can be seen that when the origin image is modulated by the microlens array, only the lines with a minimum frequency of 3 can be resolved in both horizontal and vertical directions. When the original image is modulated by the lenticular lens array, only the line pairs with the same frequency of 3 can be distinguished in the horizontal direction, and the same line pairs with the origin image can all be distinguished in the vertical direction. It is evident that the lens array effectively filters out high-frequency information, thereby displaying only low-frequency signals.

In terms of the LC lens array, the modulation of the origin image is divided into two steps. First, the

top and bottom lens arrays modulate the origin image at different moments, and then the modulation images of the two moments are synthesized into one image by time-division multiplexing. The results are shown in Fig. 3c. It can be seen that the LC lens array exhibits all-pass characteristics in both horizontal direction under the voltage-off state and vertical direction under the voltage-on state. Following time-division multiplexing, the LC lens array exhibits slight degradation in sharpness while maintaining high-frequency information.

In addition to the time-division multiplexing of the LC lens array to realize the passage of high-frequency information, the pitch of the LC lens array also affects high-frequency information in the reconstructed 3D image. According to the Nyquist sampling principle, the high-frequency information exceedingly twice the frequency of the LC lens array period is filtered out. Therefore, the smaller the pitch of the LC lens array, the higher the sampling frequency of the LC lens array will be so that higher frequency information can be passed along the period direction of the lens. Fig. 3d shows the modulation results of LC lens arrays with different pitches of 5, 10, and 20, respectively, for the origin image. The origin image also contains black and white line pairs with frequencies of 3 and 5. To demonstrate the modulation of the LC lens arrays with different pitches for low and high-frequency information, the cut-off frequency is set to 4, which is between the low and high-frequency information in the origin image. *P* is the pitch of the LC lens array. The results indicate that decreasing the pitch of the LC lens array leads to an increase in the sampling rate of the array, enabling the lens array to transmit a high frequency of 5.

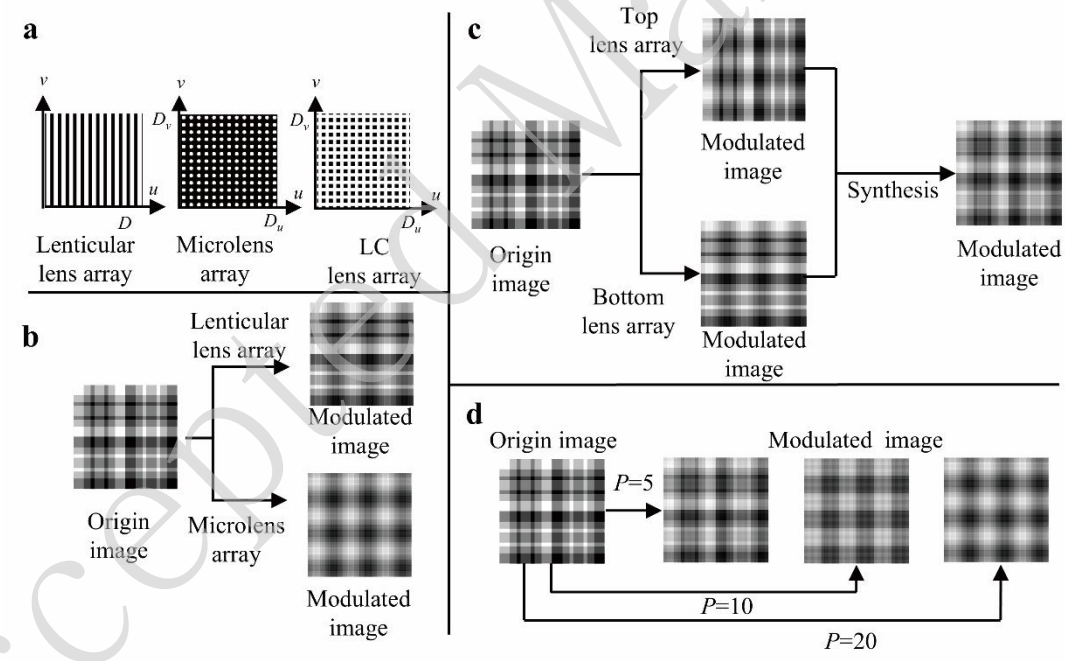

Fig. 3 Modulation results of image information at different frequencies by different types of lens arrays. a Transfer function images of the lenticular lens array, microlens array, and proposed LC lens array in the frequency domain. **b** Images modulated by a lenticular lens array with a horizontal period and a microlens array, respectively. **c** Modulated images of the proposed LC lens array at different voltage states and the final modulated image synthesized from the modulated images in the two voltage states. **d** The modulation results of the origin image by the LC lens arrays with varying pitches.

Parallax-separated pixel encoding method

In the light field 3D display, it is necessary to collect information about the 3D object from multiple angles and then process all the information into a 2D image called EIA. This process requires encoding sub-pixels in the parallax image array captured by the digital camera array according to the structure of the LC lens array and the relative positions of the lens array and the 2D display, named pixel encoding. The relative positions of the LC lens array and the 2D display in the proposed 3D display are shown in Fig. 4a, where l_p is the sub-pixel short side length and the aspect ratio of the sub-pixel is 3:1. In the 2D display, the sub-pixels are arranged in RGB strips. Both the top and the bottom LC lens arrays are placed at an angle φ with respect to the 2D display in order to avoid the moiré patterns.

In order to reconstruct a 3D image with full parallax, the proposed light field 3D display reconstructs 3D images by displaying EIAs containing parallax with different directions through the proposed LC lens array in a time-division multiplexing scheme. Therefore, a parallax-separated pixel encoding method is proposed. First, parallax image arrays containing horizontal and vertical parallaxes are acquired separately, scaled to the same image size as the EIA, and encoded. The parallax image index s determines the parallax image index corresponding to each sub-pixel of the EIA. This determination is based on the relative positions of the LC lens array and the 2D display. At different moments of t_{off} and t_{on}, different layers of the lens array in the LC lens array modulate the light, resulting in different relative positions of the lens array and the 2D display. The 2D display exhibits different EIAs at different moments, and the parallax image index s corresponding to each sub-pixel is also changed. After the parallax image indices of all sub-pixels in the EIA are obtained, the sub-pixels at the same position in the corresponding parallax image are then extracted and filled into the EIAs, resulting in the EIAs containing the horizontal and vertical parallaxes, respectively.

The EIA generation process at t_{off} moment is shown in Fig. 4b, when the PCL is in the voltage-off state, the digital camera acquires the parallax information in the horizontal direction, obtains the parallax image array, and scales the image size. The parallax image index of $s_{j,k}$ corresponded to the (j, k)th sub-pixel of the EIA is given by

$$s_{j,k} = \left\lfloor \frac{\left\{ [j-1+3(k-1)\tan\varphi] \bmod \dfrac{P}{l_p \cos\varphi} \right\} Sl_p \cos\varphi}{P} \right\rfloor \tag{12}$$

where P denotes the pitch of the top and bottom LC lens arrays and S denotes the total number of parallax images. J and K denote the total number of columns and rows of pixels for the EIA, respectively. According to the parallax image index $s_{j,k}$, the sub-pixel in the $s_{j,k}$th parallax image is extracted to fill in the corresponding (j, k)th sub-pixels in the EIA, and thus obtains the EIA containing horizontal parallax. At t_{on} moment, when the PCL is in the voltage-on state, the scaled parallax image array with vertical parallax is obtained. The parallax image index corresponding to each sub-pixel in the EIA is changed. The parallax image index of $s_{j,k}$ corresponded to the (j, k)th sub-pixel of the other EIA is calculated as

$$s_{j,k} = \left\lfloor \frac{\left\{ [(J-j)\tan\varphi + 3(k-1)] \bmod \dfrac{P}{l_p \sin\varphi} \right\} Sl_p \sin\varphi}{P} \right\rfloor \tag{13}$$

After filling the sub-pixel information according to the parallax image index, the EIA containing

vertical parallax is also obtained. The EIAs of different moments are time-division multiplexed by adjusting the voltage state of the PCL layer, thus reconstructing a full-parallax 3D image.

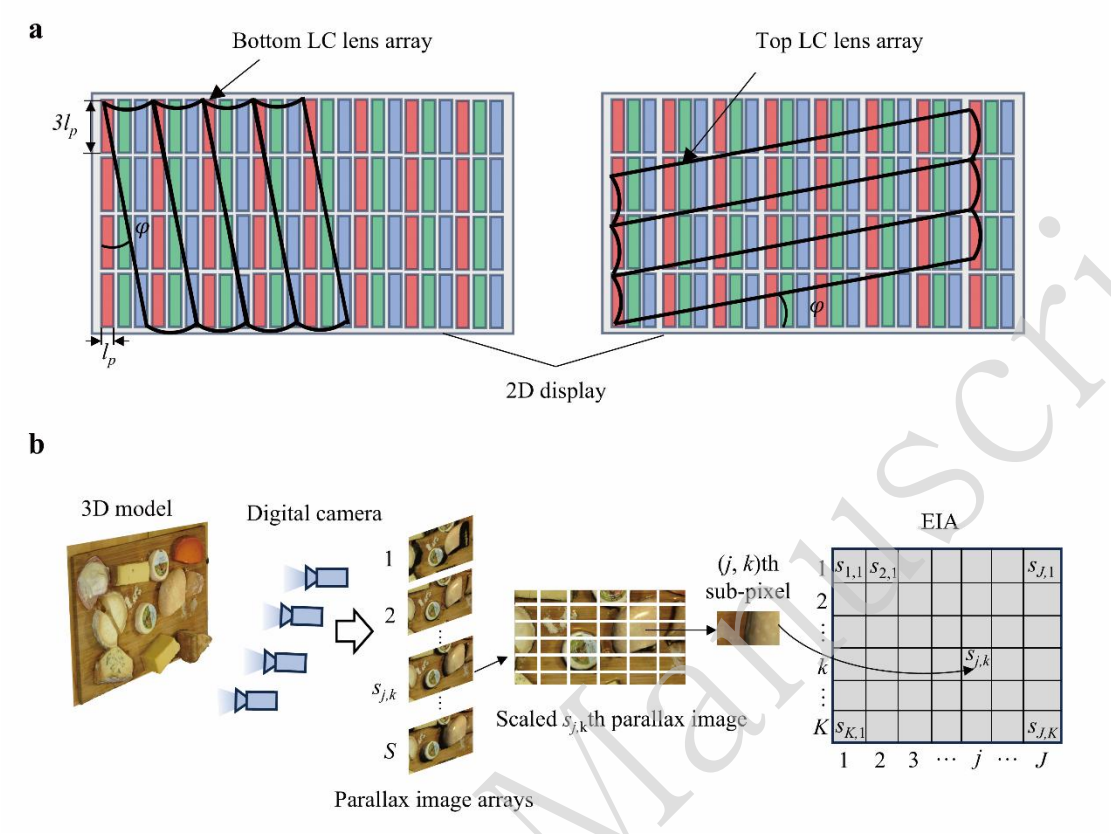

Fig. 4 Schematic diagram of the cooperation between the LC lens array and the 2D display. a Schematic diagram of the position of different layers of LC lens array relative to the 2D display. **b** Schematic diagram of the EIA generation process at t_{off} moment.

Results

In order to verify the modulation performance of the proposed LC lens array, a computer simulation is used to simulate the distribution of the LC molecules in the LC lens array under different voltage states. Figs. 5a and 5b show the cross-sectional view of the LC molecule's direction distribution within the LC layers at voltage-off and voltage-on states. A linearly polarized light is incident parallel or perpendicular to the alignment direction, and the refractive index is unchanged. In the voltage-on state, non-uniform spatial electric field distribution will be generated between planar electrodes and rectangular electrodes. As a result, the LC molecules will maintain larger inclination angles in the boundaries than those at the center of the LC lens array. Thus, the LC lens array with gradient refractive index distributions is generated between two LC layers, forming a focusing effect on the linearly polarized light whose polarization direction is parallel to the LC molecules. Based on the values of the inclination angle of the LC molecule in Fig. 5b and Equation (1), the refractive indices of the extraordinary ray of the proposed LC lens array are calculated at V_{on} = 6V. The refractive index distribution of each LC lens is centrosymmetric, and the maximum refractive index difference is 0.18, as shown in Fig. 5c. It is noteworthy that there is a sudden change in refractive index at the edge of each LC lens. This is caused by a change in the inclination angle of the LC molecules above the

electrode, but this area is only a few micrometers and has no effect on the overall focusing effect. We can obtain the focusing effect of the LC lens array from Fig. 5d. The phase difference of each LC lens exceeds 28π, and the phase distribution of the proposed LC lens array matches well with that of an ideal lens, indicating that the proposed LC lens array has a good focusing effect.

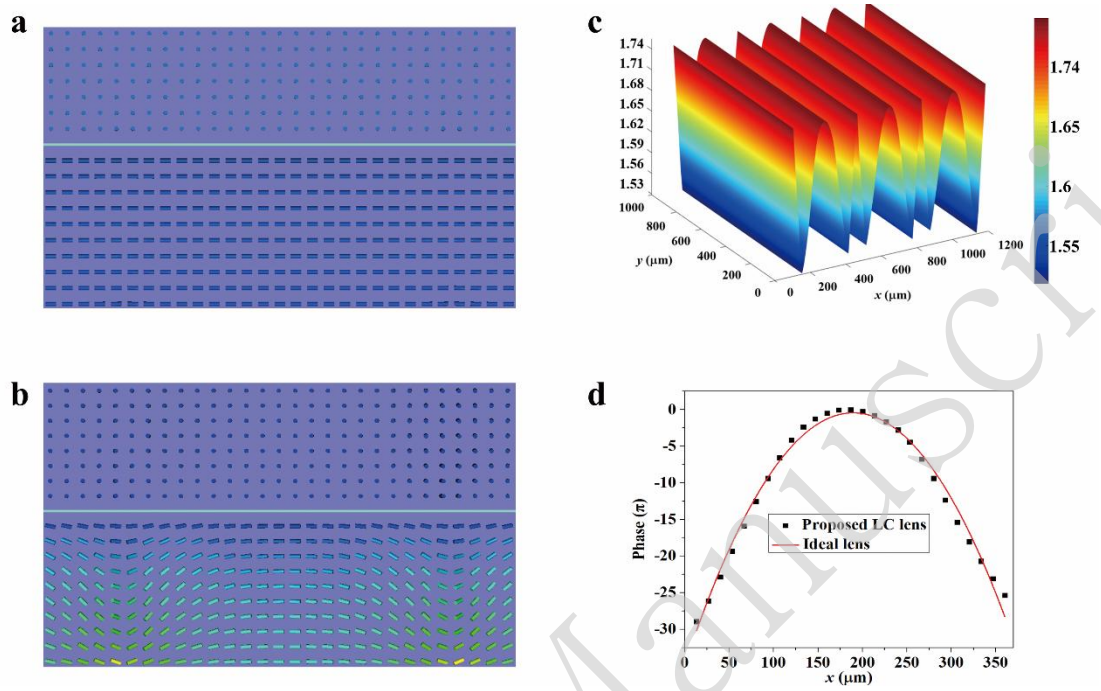

Fig. 5 Simulation results and performance testing of LC lens array. a Simulated cross-sectional view of the LC molecules director distribution at V_{on} = 0V. **b** Simulated cross-sectional view of the LC molecules director distribution at V_{on} = 6V. In V_{on} = 0V state. **c** Refractive index distribution of the proposed LC lens array at V_{on} = 6V. **d** Phase difference for the extraordinary ray of the proposed LC lens array at V_{on} = 6V.

Figs. 6a and 6b show the optical experiment results of the LC lens array presenting the horizontal direction focusing effect and vertical direction focusing effect under the control of the PCL. When the PCL is in the voltage-off state, the LC lens array has a focusing effect in the horizontal direction. When the PCL is in the voltage-on state, the focusing effect of the LC lens array exhibits in the vertical direction. To test the switching time of the PCL, the PCL is positioned beneath the linear polarizer, and light with the same polarization direction as the linear polarizer is injected from below the PCL. When a voltage is applied to the PCL, the LC molecules within it are uniformly distributed. The direction of the incident light's polarization remains unchanged, and the light passes completely through the linear polarizer. When the applied voltage to the PCL is canceled, the LC molecules within it are distorted. The polarization direction of the incident light is rotated by 90°, and the light cannot pass through the linear polarizer.

Chromatic aberration is a factor that cannot be avoided in the LC lens array, which affects the quality of the reconstructed 3D image. The chromatic aberration of the proposed LC lens array has been analyzed. As shown in Fig. 6c, the red line indicates the red light, the green line indicates the green light, and the blue line indicates the blue light. When the driving voltage increases, the value of the focal length difference of RGB trichromatic light decreases gradually. Therefore, when the driving voltage is high enough and the LC lens array is set to the shortest focal length, the focal length difference of the LC lens array for the RGB trichromatic light is almost zero.

A high switching rate is a requisite condition for the use of time-division multiplexing. It is widely recognized that the thickness of the LC layer typically ranges from tens of micrometers to one hundred micrometers to achieve an adequate phase modulation. This results in a response time that varies between a few hundred milliseconds and a few seconds[36], preventing the realization of time-division multiplexing. As for the proposed time-sequential polarization LC lens array, there is no requirement to control the on/off states of the driving voltage applied to the LC lens. The focusing and transmission effects of the LC lens are achieved by controlling the on/off of the driving voltage of the PCL. The PCL generally adopts a twisted nematic phase to solely modulate the polarization direction of incident light and has a thickness of only a few micrometers. This results in a response time that ranges from a few milliseconds. The high response time allows for a high frame rate, which in turn ensures a time-sequential 3D display with a comfortable experience because the human visual persistence limitation ranges from 0.1 s to 0.4 s. Generally, an image refresh rate exceeding 24 Hz is required for the human eye not to perceive stuttering. Fig. 6d shows the switching time of the PCL. The rise time of the light transmission rate after applying voltage is 2.16 ms, and the decay time of the light transmission rate after canceling the voltage application is 2.63 ms, which indicates the switching frequency can reach about 208 Hz, thus enabling time-division multiplexing of 3D images. Furthermore, the polarization conversion efficiency of PCL has been measured in different voltage states, revealing that PCL exhibits a polarization conversion efficiency of 95.9%.

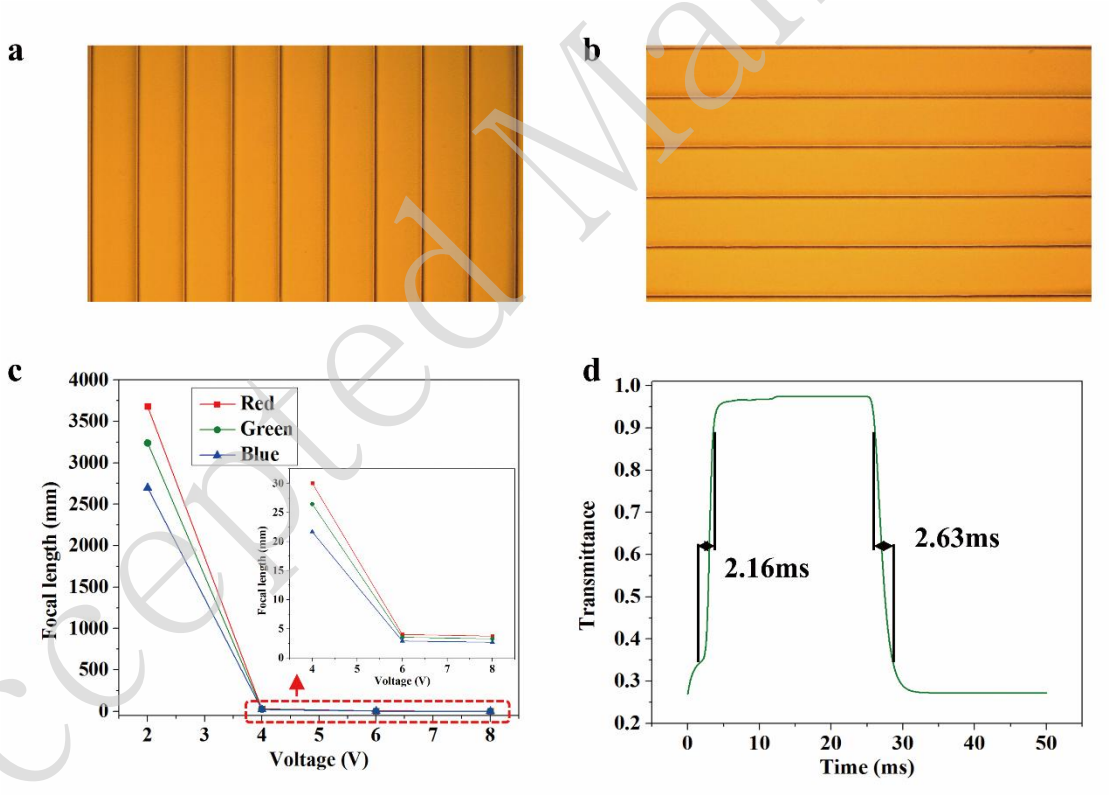

Fig. 6 Experimental results of the LC lens array. a Horizontal direction focusing effect of the LC lens array at the voltage-off state. **b** Vertical direction focusing effect of the LC lens array at the voltage-on state. **c** Focal distance of the LC lens array for the RGB trichromatic light under different voltages. **d** Switching time of the PCL.

The light field uniformity of three types of lens arrays is analyzed. The light field uniformity is represented by the variance between the overall light field illuminance and the average light field

illuminance. The illuminance distributions on the image plane of these light field 3D displays are shown in Figs. 7a, 7b and 7c. After normalization, the variance of the 3D display based on the lenticular lens array is 0.838. The variance of the 3D display based on the microlens array is 0.837. In the proposed 3D display, the variance is 0.829. Comparative result reveals that the light field uniformity of all three types of 3D displays is comparable. This consistency stems from the uniform 360 μm-pitch employed across all types of lens arrays employed. The pitch and imaging quality of the lens array are the primary factors influencing light field uniformity. The small pitch lens structure inherently promotes uniform light field distribution. The modulation effect of lens units in three types of lens arrays on the light source is illustrated in Figs. 7d, 7e and 7f. Curves of different colors represent the modulation effects of several adjacent lens units on the light source. The densely packed small-pitch lens array can modulate the Gaussian light source into a flat-top light source, thereby achieving uniform light field distribution. When the lens array pitch increases, light field uniformity will significantly decrease. The brightness uniformity of the proposed 3D display is also measured, revealing a 16.5% reduction in brightness at the darkest edge of the employed 2D display compared to the brightest center point, and an 18.6% reduction in brightness at the edge compared to the center for the proposed light field 3D display. This demonstrates that the proposed time-sequential LC lens array does not compromise the light uniformity inherent to the original 2D display.

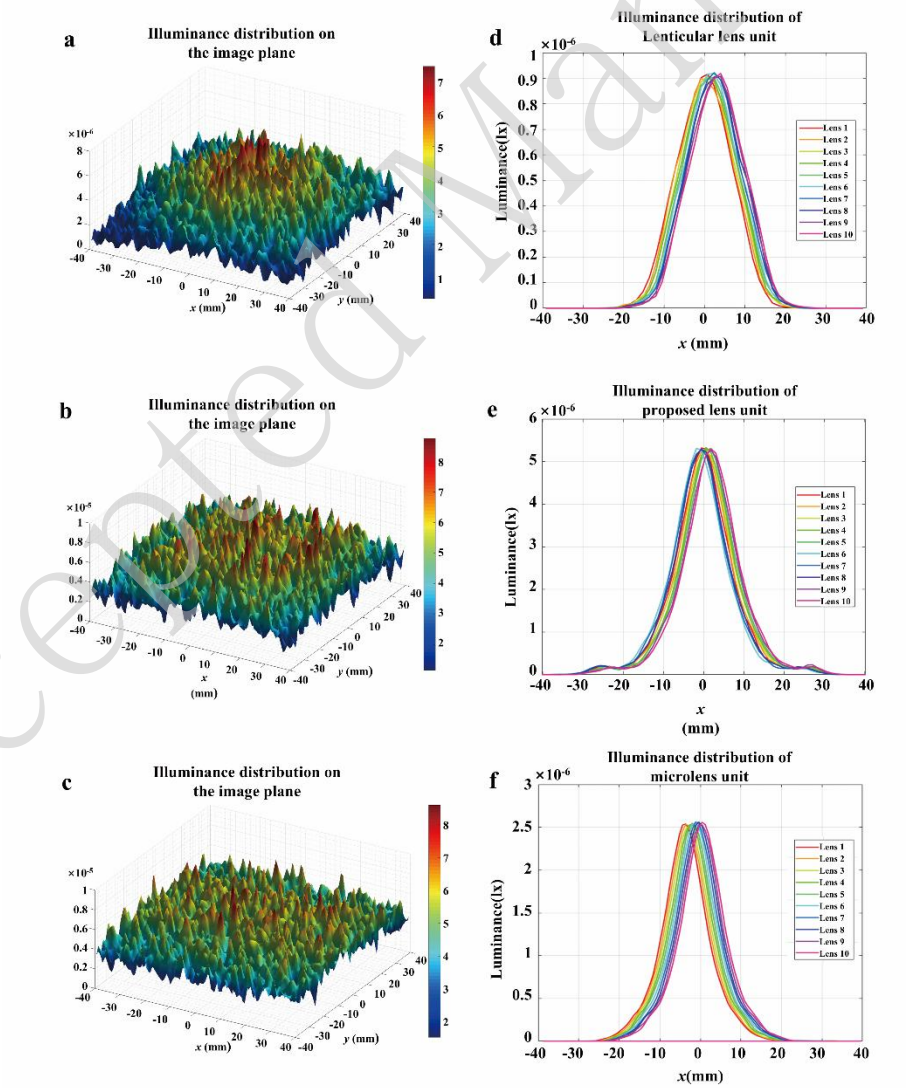

Fig. 7 Simulation results of illuminance distribution. a Illuminance distribution on the image plane of the lenticular lens array. **b** Illuminance distribution on the image plane of the proposed lens array. **c** Illuminance distribution on the image plane of the microlens array. **d** Illuminance distribution of the lenticular lens unit. **e** Illuminance distribution of the proposed lens unit. **f** Illuminance distribution of the microlens unit.

The luminance and optical efficiency of the proposed light field 3D display are measured. The employment of a nine-point measurement method with the use of a luminance meter has revealed that the 2D display exhibits an average brightness of 838.6 nits, while the proposed light field 3D display exhibits an average brightness of 554.7 nits. The total transmittance of the time-sequential LC lens array is 66.15%. The transmittance of each layer in the time-sequential LC lens array is also analyzed. For incident light aligned with the LC lens's direction, the transmission rate of a single-layer LC lens array is 88.1%. For incident light perpendicular to the LC lens's direction, the transmission rate of a single-layer LC lens array is 89.2%. The time-sequential LC lens array exhibits greater brightness attenuation compared to the sum of attenuation of two single-layer LC lens arrays. The reason lies in the presence of air between the two layers of the LC lens array. As a low-refractive-index medium, air may cause total internal reflection when incident light passes from the bottom LC lens array into the air medium, resulting in reduced brightness. Additionally, dust particles suspended in the air scatter the incident light, leading to greater light attenuation. This issue can be resolved by filling the gap between the two single-layer LC lens arrays with the high-refractive-index medium. The high-refractive-index medium reduces the refractive index difference between the medium and the LC lens array, thereby decreasing total internal reflection. Additionally, a homogeneous medium can effectively minimize brightness attenuation caused by scattering.

To demonstrate the depth and parallax of the reconstructed 3D image, the letters “AB” have been used as a 3D model for 3D image reconstruction. The results are shown in Fig. 8a, which shows the reconstructed 3D image of the letter “AB” at different angles. The horizontal and vertical viewing angles of the proposed light field 3D display are both 12.5° due to the limitation of the pitch and thickness of the LC lens array. The experimental results show that the reconstructed 3D image has correct parallax in both horizontal and vertical directions. Some “desserts” are also used as the target 3D model, and the reconstructed 3D image is shown in Fig. 8b. The reconstruction results for the “desserts” demonstrate that the reconstructed 3D image has high resolution and distinct surface texture while having full parallax.

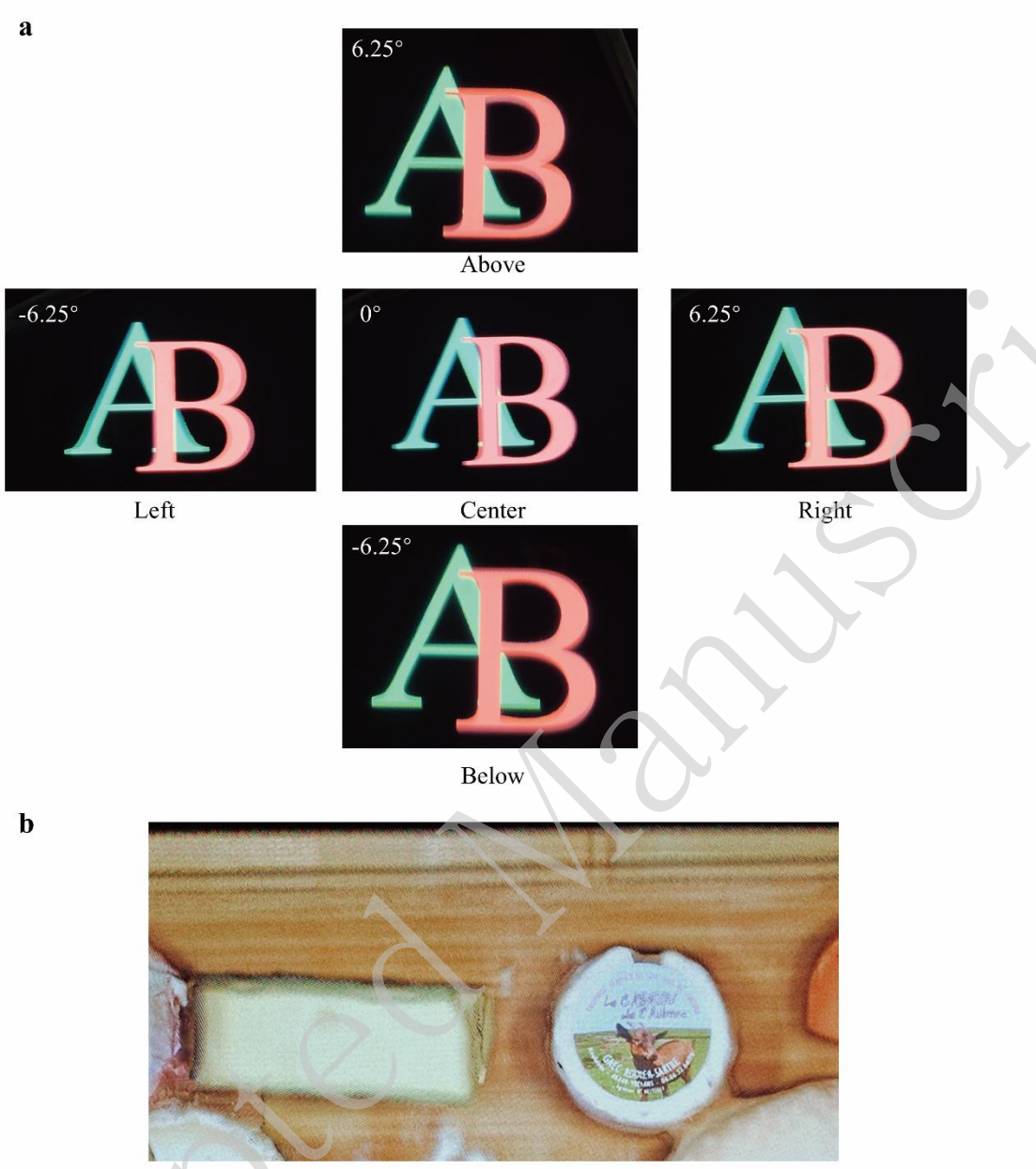

Fig. 8 Reconstructed 3D image of the proposed light field 3D display. a Reconstructed 3D image of the 3D model comprising an "A" and a "B" from multiple positions along the horizontal direction (Visualizations 1) and the vertical direction (Visualizations 2), respectively. **b** Reconstructed 3D image of the 3D model of "desserts".

In order to verify that the proposed LC lens array has higher resolution after time-division multiplexing, an optical imaging comparative experiment is conducted for the 3D images reconstructed based on the proposed lens array, lenticular lens array, and microlens array. The materials of the three lens arrays are liquid crystals. The pitches of three types of lens arrays are all 360 μm. The focal lengths of the lenticular lens array and microlens array are both 3mm. To ensure that the image planes of the top and bottom LC lens arrays are in the same position, the focal length of the bottom lens array is 3mm and that of the top lens array is slightly larger than 3mm. The dessert with text is used as the target for 3D reconstruction, and its ground truth is shown in Fig. 9a. The results of the comparative experiment are presented in Figs. 9b - 9d. Fig. 9b shows that the 3D image obtained using the proposed

LC lens array and following time-division multiplexing of two 3D images with different parallaxes. It can be seen that the four letters of "GAEC" in the 3D image can be easily distinguished. The 3D image reconstructed using the lenticular lens array has a lower resolution, which is proved by the fact that the three lines in the letters of "E" are indistinguishable in Fig. 9c. In Fig. 9d, the reconstructed "GAEC" using the microlens array is almost indistinguishable. The analysis of the results reveals that the 3D images reconstructed by the proposed LC lens array after time-division multiplexing are smoother and have a higher resolution than the 3D images reconstructed by the lenticular lens array and microlens array.

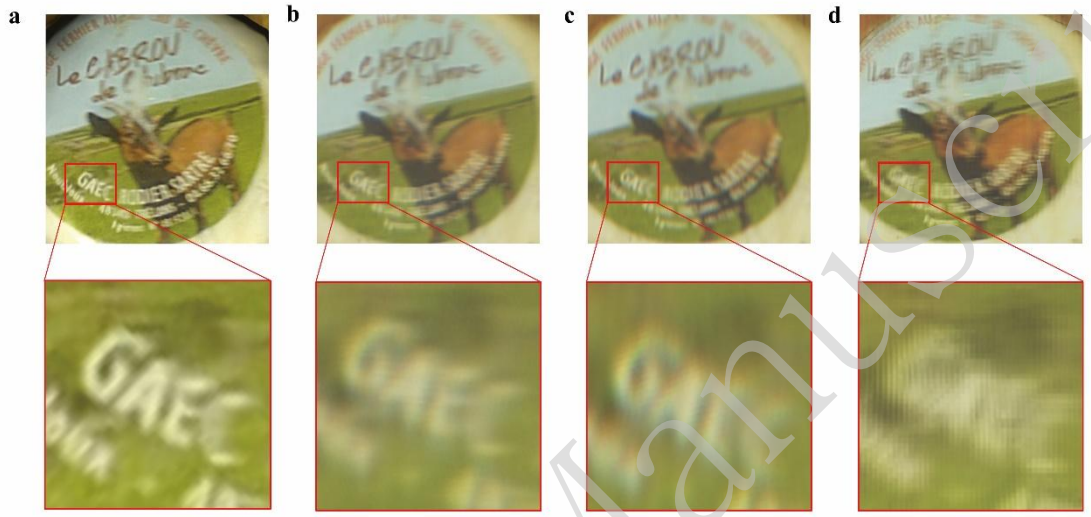

Fig. 8 Comparison of 3D images reconstructed by different types of lens array. a Ground truth of the 3D model **b** 3D image reconstructed based on the proposed LC lens array after time-division multiplexing. **c** 3D image reconstructed based on the lenticular lens array. **d** 3D image reconstructed based on the microlens array.

To quantitatively compare the resolution of the reconstructed 3D images using light field 3D displays with different types of lens arrays, this study measures the 3D image resolution by quantifying the resolution decay of the reconstructed 3D images relative to 2D display resolution. Fig. 10a depicts a 2000-line-pair ISO 12233 resolution test chart with 100 × magnification. The four regions—K1, J1, K2, and J2—are used to measure horizontal and vertical resolution. A camera is used to capture the displayed resolution test chart. Fig. 10b shows the image of the resolution test chart loaded on the 4K 2D display. The test results indicate that the camera's resolution for this 2D display is 1950 × 1710 lines width per picture height (LW/PH). Fig. 10c shows the resolution results of the proposed light field 3D display. After time-division multiplexing, the camera's resolution for the proposed light field 3D display is 880×880 LW/PH. Since the camera's sensor height and lens imaging capability remain unchanged, the reconstructed 3D image exhibits a 60% reduction in resolution compared to the 4K 2D display, resulting in a 3D display resolution of 1732×1265. Figs. 10d and 10e show the resolution results of the light field 3D displays based on a lenticular lens array and a microlens array, respectively. The camera's resolution for the light field 3D displays based on a lenticular lens array is 475×1180 LW/PH, corresponding to a 3D display resolution of 935×1492. The camera's resolution for the light field 3D displays based on a microlens array is 300×325 LW/PH, corresponding to a 3D display resolution of 591×411. Comparing Fig. 10c and 10d reveals that the lenticular lens array-based light field 3D display achieves a higher resolution in one direction but exhibits lower resolution in another direction. The proposed light field 3D display demonstrates higher overall resolution, although its resolution in a single direction is slightly lower than that of the lenticular lens array-based light field

3D display. As can be seen from Figs. 10c and 10e, the proposed light field 3D display has a higher resolution in both directions and reduces the ghosting phenomenon compared to the light field 3D display based on the microlens array, thereby enhancing the viewing experience of the viewer.

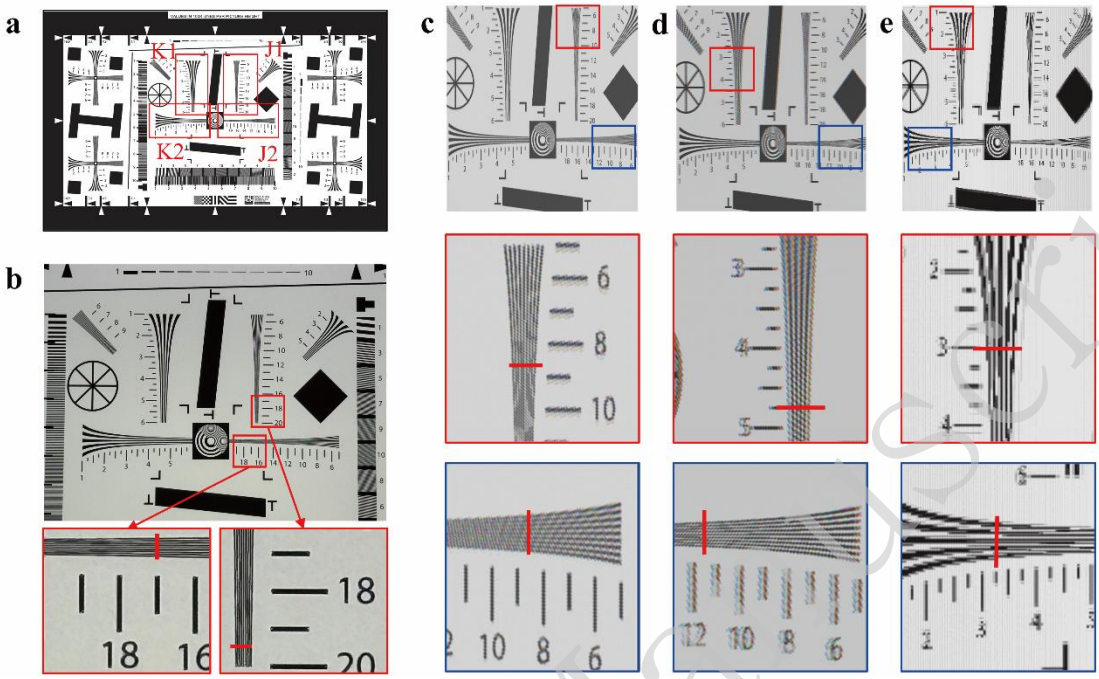

Fig. 10 Comparison of 3D image resolution reconstructed by different types of displays based on an ISO 12233 resolution test chart. a ISO 12233 resolution test chart. **b** Captured image of the resolution test chart displayed on the 4K 2D display. **c** 3D image of the proposed light field 3D display. **d** 3D image of the light field 3D display based on a lenticular lens array. **e** 3D image of the light field 3D display based on a microlens array.

The crosstalk analysis has also been conducted. For light field 3D displays, crosstalk manifests as interference between adjacent view images. Crosstalk is expressed as the ratio of luminous flux of the corresponding view image to that of the erroneous view image. The crosstalk distributions of the light field 3D displays based on three different types of lens arrays are shown in Fig. 11. Fig. 11a illustrates the crosstalk distribution of the light field 3D display based on a lenticular lens array within a single view range in the horizontal direction. The green curve represents the illuminance of the elemental image (EI) corresponding to the view image within the field of view. The red and blue curves characterize the illuminance of two adjacent EIs in the horizontal direction. Since the lenticular lens array only has focusing capability in the horizontal direction and the EIs with different parallax information are arranged horizontally, the crosstalk it receives mainly comes from the light emitted by the two horizontally adjacent EIs with different parallax information. By calculating the luminous flux of the correct view image and the erroneous view image in the horizontal direction, the crosstalk value in the horizontal direction is 14.51%.

The crosstalk distributions of the 3D display based on the time-sequential liquid crystal lens array within a single view range in the horizontal and vertical directions are shown in Figs. 11b and 11c. The proposed 3D display consists of two layers of orthogonal LC lenticular lens array, providing focusing effects only in the horizontal and vertical directions. The crosstalk of a single-view 3D image receives mainly comes from the light emitted by the two adjacent EIs with different parallax information in the horizontal or vertical direction. The crosstalk value in the horizontal direction is 20.55% and in the vertical direction is 19%. However, due to time-division multiplexing, when reconstructing 3D images

horizontally, crosstalk information generated by incorrect EIs in the vertical direction still affects the process. Therefore, the crosstalk of the proposed 3D display is higher than that of the 3D display based on the lenticular lens array.

For the light field 3D display based on the microlens array, since it uses the spherical lens as the lens units, the microlens array can refract light rays from all directions. Therefore, the crosstalk of the 3D display based on the microlens array comes from all adjacent EIs with different parallax information, as shown in Figs. 11d and 11e. The green curve represents the illuminance of the EI corresponding to the view image within the field of view. The red and blue curves characterize the illuminance of two adjacent EIs in the horizontal or vertical direction. The remaining four colors curves indicate the illuminance of EIs adjacent along the four diagonals. The crosstalk value is 23.9% in the horizontal direction and 24.44% in the vertical direction. The crosstalk of the 3D display based on the microlens array is the highest among the three 3D displays.

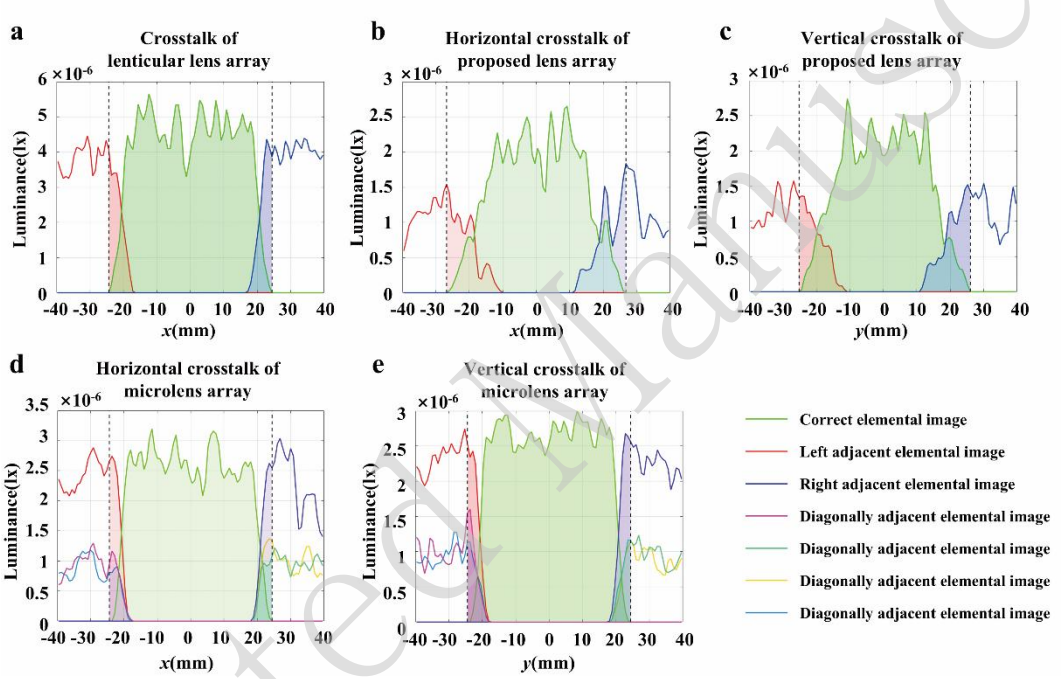

Fig. 11 Comparison of crosstalk within a single-view image reconstructed by different types of displays. a Crosstalk of the lenticular lens array. **b** Horizontal crosstalk of the proposed lens array. **c** Vertical crosstalk of the proposed lens array. **d** 3 Horizontal crosstalk of the microlens array. **e** Vertical crosstalk of the microlens array.

Additionally, since the voltage switching of the PCL cannot be perfectly synchronized with the switching of the EIA on the 2D display, the switching rates misalignment emerges. This misalignment can induce beat frequency phenomena. When the switching frequencies are misaligned, light emitted from the 2D screen passes through the incorrect LC lens array. And the 3D display will display an incorrect image. Assuming the polarization conversion layer switching frequency is f_s, and the 2D display's switching frequency for displaying horizontal and vertical EIAs is f_d. When $f_s = f_d$, the polarization conversion layer twists or maintains the polarization state of light emitted from the 2D display as the EIAs switch. The 3D images with different parallaxes are then reconstructed by the light through the corresponding lens array. When the polarization conversion layer drive or 2D display's switching frequency introduces delay, $f_s \neq f_d$. At this point, beat frequencies occur between the two frequencies, causing the 3D display to show an incorrect image with a flicker frequency of $f_p = |f_s - f_d|$. When f_p is low, the human eye perceives an erroneous image flickering. The viewer will observe the

3D image overlaid by an erroneous image flickering at frequency f_p. The human eye is most sensitive to low-frequency fluctuations between 1-10Hz, causing intense dizziness. To prevent such problems, utilizing the switching step signal from the 2D display, such as HDMI's V-SYNC or DisplayPort's Sync signal, to force the polarization conversion layer's switching rate f_s to strictly follow the 2D display's frame switching rate f_d eliminates frequency fluctuations in the driving circuit, achieving complete suppression of beat phenomena. Simultaneously, excessively high switching rates cause temperature rise, potentially accelerating material aging or molecular structural fatigue. Therefore, to align with existing 2D display switching rates and enhance viewer comfort, PCL switching frequencies are controlled between 60Hz and 120Hz—the current mainstream refresh rates for 2D displays. At this operating frequency, both PCL durability and visual comfort for the human eye are effectively ensured.

Discussion

In this study, we propose a full-parallax high-resolution light field 3D display based on a time-sequential polarization LC lens array to achieve the reconstruction of high-resolution and full-parallax 3D images. However, our current 3D displays only achieve 3D image reconstruction in the horizontal and vertical directions, while parameters such as depth of field and viewing angle remain limited. Our next step is to enhance the degree of freedom in light field control devices, thereby further addressing the mutual constraints among various parameters in 3D displays. Focal length significantly impacts the display quality of reconstructed 3D images. We aim to investigate how to optimize 3D display performance by leveraging the adjustable focal length of liquid crystal lenses. For instance, implementing time-division multiplexing with a zoomable liquid crystal lens array could enhance the depth of field of reconstructed 3D images, or utilizing the variable focus capability of the liquid crystal lens array to switch 2D /3D display modes. Additionally, the meta-lens, as a new technology, possesses exceptional light field modulation capabilities and thus holds immense potential for 3D display applications. The achromatic properties of meta-lens arrays can effectively optimize aberration and chromatic aberration while maintaining polarization selectivity to ensure multi-degree-of-freedom control of the light field[37]. Furthermore, the ultra-thin nature of the meta-lens array enhances system compactness, thereby expanding the range of potential applications.

Additionally, the proposed time-sequential polarization LC lens array exerts varying degrees of influence on the performance parameters of 3D displays compared to conventional solid lens arrays. Regarding the field of view, the time-sequential dual-polarization switching function employed in this work imposes limitations on the direction of the field of view but does not significantly affect its size. The proposed time-sequential LC lens array consists of two orthogonal LC lens arrays that are sensitive to the polarization direction of incident light. Each lens array can only refract incident light with specific polarization direction. Consequently, the 3D images reconstructed by this 3D display exhibit parallax in only two directions. When viewed from other directions, the image parallax diminishes. However, the size of the field-of-view is primarily limited by the pitch and the Object distance of the LC lens array, with time-division multiplexing having a minor impact. Secondly, the prototype proposed in this paper employs an LC lens array with a relatively short focal length, resulting in a limited depth for the 3D image. Additionally, potential angular coupling errors between the incident light polarization direction and the LC lens array polarization direction may slightly weaken the light-focusing performance of the LC lens array. As for the spatial resolution, a 3D image can be viewed as composed of numerous voxels in space. Each voxel is composed of pixels at the same

position under different lens units. For a 2D display with fixed pixel size and pixel number, a smaller lens array pitch means fewer pixels covered per lens unit, while a larger number of the total lens units. A higher number of lens units increases the number of pixels of a voxel, thereby enhancing spatial resolution. However, fewer pixels covered per lens unit reduces the total number of viewpoints, diminishing the motion parallax of the reconstructed 3D image. To balance these competing effects on 3D display performance, we ultimately selected three distinct types of lens arrays with a 360μm-pitch for comparative testing. Research on enhancing 3D display effects through computational techniques is currently a hot topic. Methods such as image pre-correction or ray tracing can process captured information to improve 3D display performance, including depth resolution and spatial resolution. We will also explore the potential applications of computational techniques in enhancing 3D display performance in the future.

Conclusion

We propose a full-parallax high-resolution light field 3D display based on a time-sequential polarization LC lens array. The 3D image with a high resolution in one direction is reconstructed in different stages by using the time-sequential polarized LC lens array, and then 3D images are time-division multiplexed to reconstruct a full-parallax high-resolution 3D image. The experimental results confirm that the proposed 3D display can reconstruct high-resolution 3D images with horizontal and vertical parallaxes. The resolution of the proposed light field 3D display is 1732×1265, which is higher than those of the light field 3D displays based on the conventional lenticular array and microlens array with the same lens parameters. The anisotropy of the LC lens array helps to achieve high-speed polarization conversion and 3D image reconstruction in different directions. The high switching speed of the PCL and lightweight construction make it a more suitable choice for common display applications than other time-division multiplexing methods. However, the durability of time sequential LC lens array under high-frequency conditions and the potential for viewer dizziness are still challenges for the proposed light field 3D display. Additionally, our subsequent work will focus on further leveraging the properties of the liquid crystal lens array or utilizing new technologies such as meta-lens to enhance other parameters of 3D displays, such as viewing angle and depth of field. Additionally, extending the service life of 3D displays and enhancing viewing comfort are also matters in our future work, which can elevate the practical application value of the light field 3D display.

Materials and methods

Fabrication of the liquid crystal lens array. The proposed time-sequential LC lens array is fabricated using conventional alignment and encapsulation processes. Planar indium tin oxide (ITO) electrodes are sputtered and etched on a glass substrate, followed by spin-coating of the alignment material polyimide (PI). This process is repeated on four layers of glass substrates. A liquid crystal mixture is then injected into the cell and homogeneous alignment is induced by the buffed layers. The low viscosity E7 liquid crystals are used to fabricate the LC lens arrays. The dielectric anisotropy $\Delta\varepsilon$ is 11.4. When the incident light is λ = 589 nm, the unusual refractive index n_e is 1.741, the usual refractive index n_o is 1.517, and the optical birefringence Δn is 0.224. The rotational viscosity γ of the LC material is 29 mPa•s. The width w of the strip-patterned electrode is 10 μm, and the pitch p of the LC lens array is 360 μm.

System composition and drivers. The system consists of a 15.6-inch 2D display, the time-sequential LC lens array, and a power supply. The 2D display is produced by BOE with the type of NE156QUM-N6C, featuring a resolution of 3840×2160 pixels and a refresh rate of 60Hz. The 2D display is connected to the computer via a high-definition multimedia interface (HDMI) cable, and the EIAs' switching rate is controlled through the OpenCV. The LC lens array is driven by two LC signal drivers. The top LC lens array and bottom LC lens array are driven by square wave signals with a frequency of 1 kHz. The polarization conversion layer is driven by square wave signals with a frequency of 60 Hz.

Data availability statement

Data underlying the results presented in this paper are not publicly available at this time but may be obtained from the authors upon reasonable request.

Acknowledgements

This work is supported by the National Key Research and Development Program of China under Grant No. 2023YFB3611500, the National Natural Science Foundation of China under Grant Nos. 62335002 and 62375009.

Author contribution

X. R. W., F. C. and Q. H. W. conceived the idea. X. R. W. and Y. X. designed the entire system, performed the simulation and conducted the experiment. X. R. W., X. Y. L., Y. J. L. and W. Z. L. undertook the experiments.

Conflict of interest

The authors declare no conflicts of interest.

References

1. Nam, D. et al. Flat panel light-field 3-D display: concept, design, rendering, and calibration. *Proceedings of the IEEE* **105**, 876-891 (2017).
2. Huang, T. Q. et al. High-performance autostereoscopic display based on the lenticular tracking method. *Optics Express* **27**, 20421-20434 (2019).
3. Li, Y. et al. Ultracompact multifunctional metalens visor for augmented reality displays. *Photonix* **3**, 29 (2022).
4. Guo, X. et al. Real-time dense-view imaging for three-dimensional light-field display based on image color calibration and self-supervised view synthesis. *Optics Express* **30**, 22260-22276 (2022).
5. Xing, Y. et al. Integral imaging-based tabletop light field 3D display with large viewing angle. *Opto-Electronic Advances* **6**, 220178 (2023).
6. Chu, F. et al. Multi-view 2D/3D switchable display with cylindrical liquid crystal lens array. *Crystals* **11**, 715 (2021).
7. Liu, Y. J. et al. High-resolution integral imaging display using targeted optimized compound lens array for voxel aliasing elimination. *Laser & Photonics Reviews* **18**, 2400182 (2024).
8. Fan, H. Z. et al. Super multi-view three-dimensional display based on near-eye

timing-polarization-characteristics apertures. *Chinese Journal of Liquid Crystals and Displays* **37**, 647-653 (2022).

9. Takaki, Y., Tanaka, K. & Nakamura, J. Super multi-view display with a lower resolution flat-panel display. *Optics Express* **19**, 4129-4139 (2011).
10. Maruyama, K. et al. A 3-D display pipeline from coded-aperture camera to tensor light-field display through CNN. Proceedings of the 2019 IEEE International Conference on Image Processing (ICIP). Taipei, China: IEEE, 2019, 1064-1068.
11. Wetzstein, G. et al. Tensor displays: compressive light field synthesis using multilayer displays with directional backlighting. *ACM Transactions on Graphics* **31**, 80 (2012).
12. Zhang, H. L. et al. Integral imaging-based 2D/3D convertible display system by using holographic optical element and polymer dispersed liquid crystal. *Optics Letters* **44**, 387-390 (2019).
13. Takaki, Y. & Nago, N. Multi-projection of lenticular displays to construct a 256-view super multi-view display. *Optics Express* **18**, 8824-8835 (2010).
14. Wetzstein, G. et al. Compressive light field displays. *IEEE Computer Graphics and Applications* **32**, 6-11 (2012).
15. Wang, P. R. et al. A full-parallax tabletop three dimensional light-field display with high viewpoint density and large viewing angle based on space-multiplexed voxel screen. *Optics Communications* **488**, 126757 (2021).
16. Liu, B. Y. et al. Time-multiplexed light field display with 120-degree wide viewing angle. *Optics Express* **27**, 35728-35739 (2019).
17. Hwang, Y. S. et al. Time-sequential autostereoscopic 3-D display with a novel directional backlight system based on volume-holographic optical elements. *Optics Express* **22**, 9820-9838 (2014).
18. Fan, M. et al. Cylindrical liquid crystal micro-lens array based on interdigital electrodes. *Liquid Crystals* **50**, 1921-1929 (2023).
19. Zhou, P. C. et al. Colour 3D holographic display based on a quantum-dot-doped liquid crystal. *Liquid Crystals* **46**, 1478-1484 (2019).
20. Ma, L. L. et al. Self-assembled liquid crystal architectures for soft matter photonics. *Light: Science & Applications* **11**, 270 (2022).
21. Wang, Z. et al. Single frontal projection autostereoscopic three-dimensional display using a liquid crystal lens array. *Optics Express* **28**, 1621-1630 (2020).
22. Zou, J. Y., Li, L. S. & Wu, S. T. Gaze-matched pupil steering maxwellian-view augmented reality display with large angle diffractive liquid crystal lenses. *Advanced Photonics Research* **3**, 2100362 (2022).
23. Liu, S. X., Li, Y. & Su, Y. K. Recent progress in true 3D display technologies based on liquid crystal devices. *Crystals* **13**, 1639 (2023).
24. Park, M. K. et al. Polarization-dependent liquid crystalline polymeric lens array with aberration-improved aspherical curvature for low 3D crosstalk in 2D/3D switchable mobile multi-view display. *Optics Express* **26**, 20281-20297 (2018).
25. Wang, L. et al. Large depth of range maxwellian-viewing SMV near-eye display based on a pancharatnam-berry optical element. *IEEE Photonics Journal* **14**, 7001607 (2022).
26. Zhang, D. W. et al. Cascaded chiral birefringent media enabled planar lens with

programable chromatic aberration. *PhotoniX* **5**, 17 (2024).
27. Zheng, Y. et al. Fast-zoom and high-resolution sparse compound-eye camera based on dual-end collaborative optimization. *Opto-Electronic Advances* **8**, 240285 (2025).
28. Pan, J. T. et al. Nonlinear geometric phase coded ferroelectric nematic fluids for nonlinear soft-matter photonics. *Nature Communications* **15**, 8732 (2024).
29. Wang, Z. Y. et al. Vectorial liquid-crystal holography. *eLight* **4**, 5 (2024).
30. Sun, Z. B. et al. Reducing resolution loss in naked-eye 3D display using dual ferroelectric liquid crystal shutters for time-multiplexed light-field display. *Journal of the Society for Information Display* **32**, 406-414 (2024).
31. Deng, H. et al. 2D/3D mixed frontal projection system based on integral imaging. *Optics Express* **28**, 26385-26394 (2020).
32. Huang, Y. G., He, Z. Q. & Wu, S. T. Fast-response liquid crystal phase modulators for augmented reality displays. *Optics Express* **25**, 32757-32766 (2017).
33. Wang, Y. J., Hsieh, H. A. & Lin, Y. H. Electrically tunable gradient-index lenses via nematic liquid crystals with a method of spatially extended phase distribution. *Optics Express* **27**, 32398-32408 (2019).
34. Guo, Y. Q. et al. Unidirectional collective transport of microspheres in nematic liquid crystal by electrically tunable reorientation. *Journal of Molecular Liquids* **357**, 119136 (2022).
35. Cao, S. et al. Dual convolutional neural network for aberration pre-correction and image quality enhancement in integral imaging display. *Optics Express* **31**, 34609-34625 (2023).
36. Li, R. et al. Short focal length tunable liquid crystal lenticular lens array based on fringe field effect. *Journal of the Society for Information Display* **28**, 793-800 (2020).
37. Lin, R. J. et al. Achromatic metalens array for full-colour light-field imaging. *Nature Nanotechnology* **14**, 227-231 (2019).